Comparison of MnAs layers on GaAs(113) surfaces grown by means of solid-phase epitaxy and conventional molecular-beam epitaxy

Y. Takagaki, B. Jenichen, C. Herrmann, and J. Herfort
Paul-Drude-Institut für Festkörperelektronik, Hausvogteiplatz 5-7, 10117 Berlin, Germany
(Received 7 May 2009; revised manuscript received 2 July 2009; published 28 July 2009)

Strain-dictated epitaxial orientation in MnAs layers on the A and B surfaces of GaAs(113) is investigated by comparing the growths using solid-phase epitaxy and molecular-beam epitaxy. Drastically different crystalline orientation and surface morphology are found for the layer on GaAs(113)A grown by means of solid-phase epitaxy while smooth $(1\bar{1}00)$- or $(1\bar{1}01)$-oriented layers are otherwise obtained. We show that $(21\bar{3}1)$ orientation is realized in the unconventional layer due to the minimization of the strain energy. The layer consists of structural domains associated with in-plane inclinations of the *c* axis of MnAs by about $\pm 42°$ from the $[33\bar{2}]$ direction of the substrate, giving rise to a polycrystalline surface morphology. The combination of coexisting crystal orientations is found to lack some reflection symmetries as a consequence of an asymmetry in the bonding energy.

DOI: 10.1103/PhysRevB.80.014116 PACS number(s): 68.35.Ct, 75.50.Cc

I. INTRODUCTION

The ferromagnetic material MnAs is prospective for spintronics applications[1] as it can be integrated into GaAs-based devices through epitaxy.[2,3] Injection of spin-polarized currents from a MnAs layer to a GaAs-(In,Ga)As quantum well[4,5] and accumulation of spin polarization at a MnAs-GaAs interface[6] have been demonstrated. In addition, the gigantic magnetocaloric effect in MnAs and the related compounds is attractive in application for a refrigeration method.[7]

The magnetic hard axis of MnAs is aligned along the *c* axis and so the magnetic properties of MnAs layers can be tuned by controlling the *c*-axis orientation.[8,9] Moreover, the *a*-axis lattice constant changes discontinuously by a few percent at Curie temperature $T_C(\approx 40\ °C)$, giving rise to a drastic change in the stress at the heterointerface. Hence, the electrical properties of MnAs layers can also be modified through the *c*-axis orientation by utilizing electroelastic effects.[10]

The growth of MnAs layers on GaAs is an example of the heteroepitaxy of highly dissimilar materials, where a hexagonal crystal is grown on a cubic crystal. [We illustrate the hexagonal crystal structure of MnAs in Fig. 1(a).] The epitaxial orientation of overlayers in such a situation is determined by the principle of minimizing the mismatches between the participating lattices. The degree of the uncompensated mismatches is consequently reflected in the crystal quality. As the orientation relationship in a (conventional) growth is established when the layer thickness is minimal, avoiding dangling bonds is generally more important than coinciding the lattice periods. For this reason, the layer favors to adjust the in-plane crystal symmetry to that of the substrate.

Recently, MnAs layers grown on GaAs(111)B by means of solid-phase epitaxy (SPE) have been found to possess an in-plane crystal symmetry which differs from that of the substrate.[11] If the growth is performed by molecular-beam epitaxy (MBE), the layers are (0001) oriented, where the sixfold symmetry of the layer fits well to the threefold symmetry of the substrate. In contrast, SPE gives rise to a symmetry-mismatched $(1\bar{1}00)$ or $(1\bar{1}01)$ orientation. The MnAs layers, as a consequence, comprise of six kinds of structural domains (including the possible reversal of the polarization) that result from the freedom in the *c*-axis align-

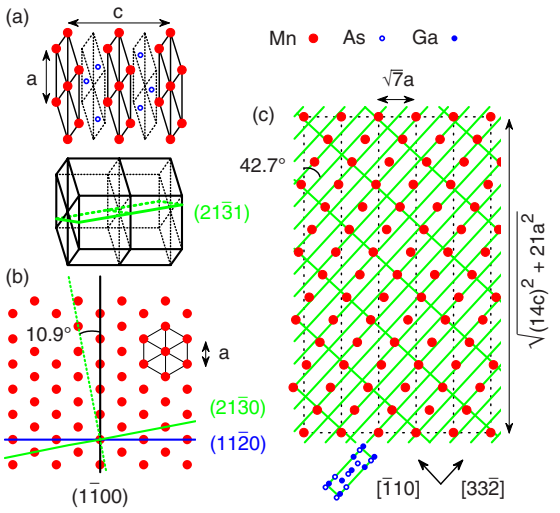

FIG. 1. (Color online) (a) Hexagonal crystal structure of MnAs. The lattice parameters in the *a*- and *c*-axis directions are *a* and *c*, respectively. The $(21\bar{3}1)$ plane is indicated in the bottom panel. (b) $(1\bar{1}00)$, $(21\bar{3}0)$, and $(11\bar{2}0)$ planes of MnAs, which is viewed here in the [0001] direction. The dotted line indicates the direction normal to the $(21\bar{3}0)$ plane. (c) Ball-and-stick model of the interface between MnAs$(21\bar{3}1)$ and GaAs(113). The large circles show the Mn atoms on the MnAs$(21\bar{3}1)$ surface. The unit cell of the $(21\bar{3}1)$ plane having sizes of $\sqrt{7}a \times [(14c)^2+21a^2]^{1/2}$ is shown by the dotted lines. The mesh of primitive cells of the GaAs(113) surface is shown by the solid lines. The primitive cell is shown using the ball-and-stick model at the bottom. The lattice mismatch is minimized in the GaAs$[33\bar{2}]$ direction when the in-plane inclination of the *c* axis is 42.7°.

ment MnAs[0001]‖GaAs$\langle 11\bar{2}\rangle$. The unusual epitaxial orientation is achieved in SPE by delaying the establishment of the orientation relationship until the layer thickness exceeds the critical value for coherent growth.[11] The elastic energy arising from the difference in the lattice periods is thus made to be dominant rather than the energy associated with dangling bonds.[12]

In this paper, we examine another case in which MBE and SPE lead to different epitaxial orientations. The MnAs layers grown on GaAs(113)A by means of SPE are $(21\bar{3}1)$ oriented. In addition, the c axis is tilted away from the high-symmetry directions of the substrate in the surface plane. The surface morphology that this high-index, low-symmetry plane produces is found to be rough. Smooth $(1\bar{1}00)$- or $(1\bar{1}01)$-oriented layers are obtained, in contrast, when the growth is carried out by MBE or on the B surface. We show that the mirror-reflection symmetries between coexisting crystal orientations in the $(21\bar{3}1)$-oriented layers are partly broken. These features can be understood in terms of the strain and bonding energies.

II. CRYSTAL GROWTH

A solid-source MBE chamber was employed to prepare MnAs layers on the Ga- and As-terminated surfaces of GaAs(113), which we refer to as the A and B surfaces, respectively. The GaAs buffer layer was grown at a substrate temperature of T_s=600 °C, where the reflection high-energy electron diffraction (RHEED) revealed a (2×8) reconstruction. The As_4/Ga beam-equivalent pressure (BEP) ratio was 18. In the MBE growth, MnAs layers were grown at T_s =250 °C. The As_4/Mn BEP ratio and the growth rate were 100 and 20 nm/h, respectively.

In a typical procedure of SPE,[11] a thin amorphous MnAs layer is deposited at a low substrate temperature. The amorphous layer is then crystallized by increasing T_s to a conventional growth temperature while the shutter of the arsenic effusion cell is closed. The arsenic-free surface is necessary for SPE to enhance the surface diffusion.[11] On a template provided in this manner, MnAs layers are further grown by MBE. We have adopted this growth recipe also in the present study. The BEP ratio was 100 for both the deposition of a 2-nm-thick layer at T_s=200 °C and the growth at T_s =250 °C. The (2×8) reconstruction of the GaAs surface prevailed even when T_s was lowered to 200 °C. We point out that RHEED exhibited a deviation from the (aforementioned) standard sequence of events for the case of the GaAs(113)A substrate, to which we will return later.

III. EPITAXIAL ORIENTATION

In Fig. 2, we show scanning-electron micrographs of the surface of the MnAs layers having thicknesses of about 50 nm. Here, the growth was carried out on the A and B surfaces simultaneously for each growth method. On GaAs(113)A, MBE produces a smooth layer, as shown in Fig. 2(a). The stripe pattern originates from alternating regions of the α and β phases of MnAs.[3] The c axis of MnAs

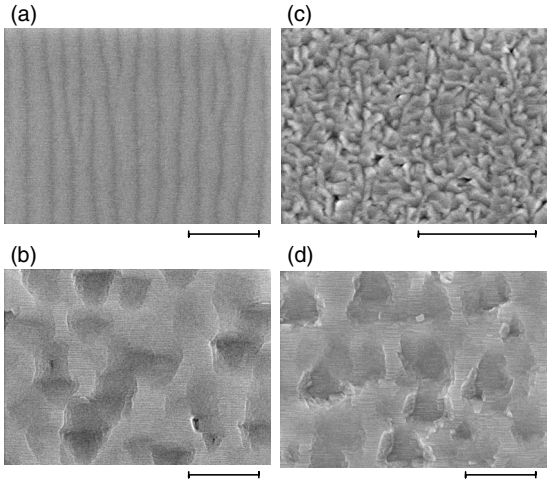

FIG. 2. Scanning-electron micrographs of MnAs layers on GaAs(113). The layers were grown by means of MBE for (a) and (b) and by SPE for (c) and (d). The substrate is orientated to be the A surface (Ga-terminated surface) for (a) and (c) and the B surface (As-terminated surface) for (b) and (d). The thicknesses of the layers are about 50 nm. The $[33\bar{2}]$ and $[1\bar{1}0]$ directions of the substrates are aligned in the vertical and horizontal directions, respectively. The scale bars indicate the length of 1 μm.

is thus deduced to be aligned in the $[33\bar{2}]$ direction of the substrate, which is set to be in the vertical direction in Fig. 2. In contrast, the surface of the layer grown by SPE on GaAs(113)A is grainy, as shown in Fig. 2(c). These highly contrasting surface morphologies represent the central finding of this paper.

With respect to the growth on the B surface, the GaAs buffer layer was not prepared with optimal conditions. This was inevitable as we have given priority to growing MnAs layers on the A and B surfaces under identical conditions. As a consequence, depressions emerged during the growth of the buffer layer, as shown in Figs. 2(b) and 2(d).[13,14] As far as the MnAs growth is concerned, however, the layers on GaAs(113)B are seen to be smooth in both MBE and SPE.

The x-ray diffraction (XRD) curves obtained from the MnAs layers are compared in Fig. 3. The measurements were carried out using the Cu $K\alpha_1$ radiation (wavelength 1.54 Å). The layer shown in Fig. 2(a) is found to be of the $(1\bar{1}00)$ orientation, curve a. As shown by curves b and d, the MnAs layers on GaAs(113)B are $(1\bar{1}01)$ oriented. Contrary to these ordinary orientations, we find a peculiar $(21\bar{3}1)$ orientation for the layers grown on GaAs(113)A by means of SPE, curve c. [Figure 1(b) shows the $(21\bar{3}l)$ plane. The $(21\bar{3}1)$ plane is illustrated in the bottom panel of Fig. 1(a).] The SPE growth of MnAs layers on GaAs(113)A, therefore, progresses in an unusual manner in terms of both the surface morphology and the epitaxial orientation.

One may ascribe the grainy surface in Fig. 2(c) to incomplete crystallization of the amorphous layer resulting from, for instance, small diffusion of the species. Based on this possibility, it was speculated in Ref. 12 that the layer consisted of microcrystallites. However, the evolution of the RHEED pattern during the preparation of the MnAs layer,

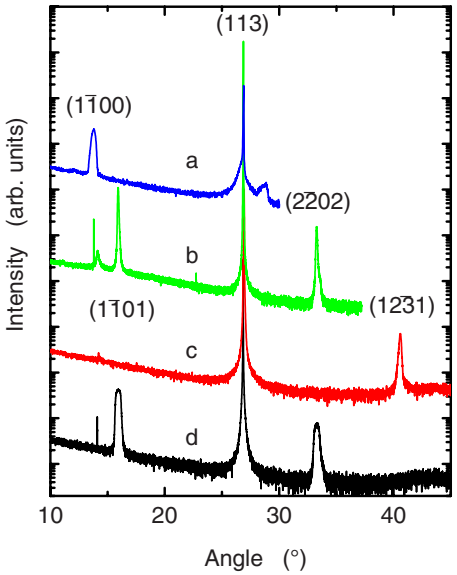

FIG. 3. (Color online) X-ray diffraction curves (ω-2θ scan) of MnAs layers on GaAs(113). Curves *a* and *b* correspond to the layers grown by MBE, whereas curves *c* and *d* are obtained from the layers grown by means of SPE. The layers were prepared on the A surface for curves *a* and *c* and on the B surface for curves *b* and *d*. The three- and four-index notations refer to GaAs and MnAs, respectively. The thickness of the layers is 50–55 nm. The curves are offset for clarity.

which we recorded in a separate growth run, appears to rule out such an explanation. For the SPE procedure on GaAs(113)A, the RHEED pattern from the GaAs buffer layer vanished at the early stage of the MnAs deposition at T_s =200 °C. This indicates complete coverage of the surface of the substrate by the amorphous layer. However, a RHEED pattern that originated from the hexagonal MnAs structure was already faintly visible at the end of the deposition of the nominally 2-nm-thick layer (not shown), suggesting a large diffusion on the GaAs(113)A surface.

In Fig. 4, we show the RHEED pattern after the MBE growth of a 150-nm-thick MnAs layer. [The surface morphology of this layer was similar to that shown in Fig. 2(c).] Apart from an increase in the intensity, the RHEED pattern did not change essentially during the solid-phase crystallization procedure and growth of the 150-nm-thick layer. The RHEED spots in Fig. 4 are strong. Moreover, their pattern can be nearly entirely associated with a single crystalline

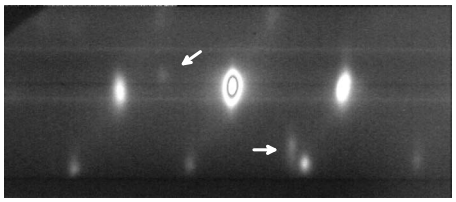

FIG. 4. Reflection high-energy electron-diffraction pattern along the [$\bar{1}$10] azimuth of GaAs(113)A. The image was taken after the MBE growth of a 150-nm-thick MnAs layer on a template prepared by SPE. All the spots apart from those indicated by the arrows are expected to be associated with a single crystal orientation.

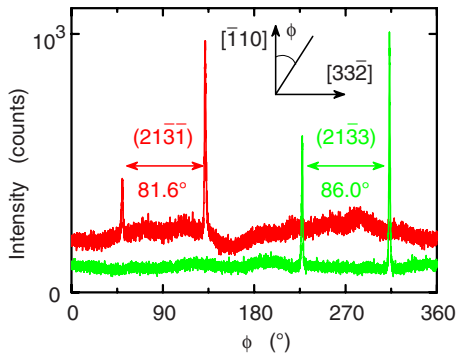

FIG. 5. (Color online) Skew geometry ϕ scan of the (21$\bar{3}\bar{1}$) and (21$\bar{3}$3) reflections of a MnAs layer on GaAs(113)A grown by means of solid-phase epitaxy. The azimuthal rotation angle ϕ is defined with respect to the azimuth of the GaAs[$\bar{1}$10] direction, as shown in the inset.

alignment in the MnAs layer. [Two features that are attributed to additional crystal orientations and/or alignments are marked by arrows in Fig. 4. The XRD curve of this layer (not shown) revealed a tiny (0004)-reflection peak, which is plausibly responsible for these extra RHEED spots.] These characteristics are unlikely to be attributable to microcrystallites.

The polycrystallike roughness of the surface, in fact, originates from structural domains. In Fig. 5, we show the ϕ scan of the (21$\bar{3}\bar{1}$) and (21$\bar{3}$3) reflections of MnAs in a skew geometry. The *c* axis in two different domains is found to be inclined by about ±42° with respect to the GaAs[33$\bar{2}$] direction in the surface plane. We emphasize that no counterparts at the 180°-rotated positions of the peaks were detected for each reflection. [The 180° shift of the peaks between the two curves is expected for the (21$\bar{3}\bar{1}$) and (21$\bar{3}$3) reflections.] It is noteworthy that the (1$\bar{1}$00)- and (1$\bar{1}$01)-oriented MnAs layers on GaAs(111)B prepared by SPE also develop a grainy surface morphology due to the coexistence of structural domains arising from the freedom in the *c*-axis alignment.[11] While this domain structure gives rise to a threefold-symmetric anisotropy in the morphology,[10] no symmetry is noticed for the surface feature shown in Fig. 2(c). The latter is presumably due to the absence of rotation symmetry among the coexisting crystal orientations revealed by the ϕ scans.

The unusual crystal orientation is intriguing not only as an unexpected epitaxial orientation but also from the viewpoint of the material properties. That is, the coexistence of the different in-plane crystal orientations effectively lowers the phase-transition stress at T_C.[10] As a consequence, the temperature interval for the coexistence of the α and β phases is reduced, as reported in Ref. 10. Spin injection at the interface between a ferromagnetic metal and a semiconductor is also influenced by the epitaxial orientation of the ferromagnetic crystal.[15] The dependence arises through the anisotropic shape of the spin bands at the Fermi level in metals (spin-filter effect) (Ref. 16) and/or the strain-induced band modification.[10]

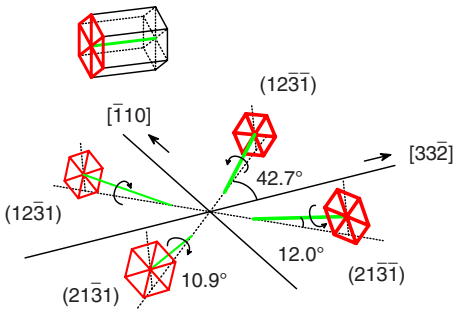

FIG. 6. (Color online) Epitaxial orientation relationship together with the tilt angles that characterize the crystal orientation. The basal plane of MnAs and the *c* axis, which are shown in the inset, are illustrated here for each crystal orientation. The arrows indicate the direction of the rotation of the basal plane around the *c* axis. The three- and four-index notations refer to GaAs and MnAs, respectively.

IV. (21$\bar{3}$1)-ORIENTED LAYER

A. Lattice mismatch

As expected for SPE-grown layers, the (21$\bar{3}$1) orientation with the in-plane inclination turns out favorable in terms of the strain energy. We illustrate the fit of atomic configurations between the MnAs(21$\bar{3}$1) and GaAs(113) planes in Fig. 1(c). Here, the circles indicate the Mn atoms and the lines represent the array of primitive cells of the GaAs(113) surface. The two lattices are seen to nearly coincide in the GaAs[33$\bar{2}$] direction when the *c* axis of MnAs is inclined by 42.7°. (The mismatch in this case is 0.16%.) In the orthogonal direction, i.e., along the GaAs[$\bar{1}$10] direction, the lattice mismatch is moderate (6.6%). Note that the atomic rows and columns on the (21$\bar{3}$1) surface that we used to estimate the mismatches are not orthogonal to each other. This nonorthogonality may lead to a deviation of the inclination angle from 42.7° if the strain energy can be further reduced.

For the (1$\bar{1}$00)- and (1$\bar{1}$01)-oriented layers that are realized in the rest of the growth cases, the *c* axis is aligned along the GaAs[33$\bar{2}$] direction.[3] The participating lattices match almost perfectly in this direction for the (1$\bar{1}$01) orientation with a mismatch of 0.2%. The corresponding mismatch is 15% for the (1$\bar{1}$00) orientation. The common mismatch in the GaAs[$\bar{1}$10] direction is 8%. The strain energy in the (21$\bar{3}$1)-oriented layer is, therefore, smaller than, or, at least, comparable to, that in the (1$\bar{1}$00)- and (1$\bar{1}$01)-oriented layers.[17] Nevertheless, for the growths by MBE and on the B surface, the energetic gain in the bonding energy appears to make the (1$\bar{1}$00) and (1$\bar{1}$01) orientations advantageous.

As one finds in Fig. 1(c), the MnAs(21$\bar{3}$1) plane is not symmetric under mirror reversals. Consequently, only the four crystal orientations displayed in Fig. 6 minimize the strain energy. (Here, the basal plane and the *c* axis are illustrated for each crystal orientation. The arrows indicate the direction of the rotation of the basal plane by 10.9° around the *c* axis.) These orientations are related to each other by mirror-reflection and rotation symmetries, i.e., the basal plane of MnAs is rotated around the *c* axis in such a way that the crystals are identical when the layer is rotated by 180° in the surface plane. However, this symmetry is broken in the actual MnAs layers, as demonstrated in Fig. 5. We have identified that the two orientations shown by thick lines in Fig. 6 exist in reality. This absence of mirror-reflection symmetry with respect to the GaAs[$\bar{1}$10] direction is the cause of the asymmetric RHEED pattern in Fig. 4.

The elimination of the other two orientations shown by thin lines in Fig. 6 is driven by the bonding energy. The GaAs(113) surface is polarized in the GaAs[33$\bar{2}$] direction, see the ball-and-stick model of the primitive cell at the bottom of Fig. 1(d). Therefore, the atomic bonds at the layer-substrate interface are not identical between the two crystal orientations associated with each of the ±42.7° tiltings despite their structural identity. The two orientations shown by the thick lines are indicated to become lower in energy than the other two due to the difference in the bonding energy. Similar selection of crystal orientation through bonding energy is known to occur for (1$\bar{1}$00)- and (1$\bar{1}$01)-oriented MnAs layers on GaAs(001). Although the lattice period is the same, the *c* axis of MnAs is aligned along either the [110] or [$\bar{1}$10] direction of the substrate depending on the growth conditions (the so-called type-A and type-B orientations).[2,3] The favored and disfavored orientations in Fig. 6 may, therefore, switch when, for instance, the stoichiometry of the amorphous MnAs layer is varied.

In general, high-index planes are not suitable for the growth plane due to their instabilities. The surface free energy is approximately given by the density of broken bonds.[18] Thus, a dense plane is generally stable as many bonds are formed within the surface plane, resulting in a small number of broken bonds that stick out of the surface plane. In Table I, we compare the areal density of Mn atoms in the (1$\bar{1}$00), (11$\bar{2}$0), (0001), (1$\bar{1}$01), and (21$\bar{3}$1) surfaces. Although the surface free energy of the high-index (21$\bar{3}$1) surface is thus expected to be high, we do not observe a facet formation during the MnAs growth. The absence of faceting may be attributed to a small diffusion on the MnAs surface, which is not surprising due to the low growth temperature.

B. Magnetic properties

As a confirmation of the unusual epitaxial orientation, we have examined the direction of the magnetic easy and hard

TABLE I. Areal density of Mn atoms in the (1$\bar{1}$00), (11$\bar{2}$0), (0001), (1$\bar{1}$01), and (21$\bar{3}$1) surfaces.

	(1$\bar{1}$00)	(11$\bar{2}$0)	(0001)	(1$\bar{1}$01)	(21$\bar{3}$1)
Areal density (10^{18} m^{-2})	9.3	5.4	8.4	4.1	1.7

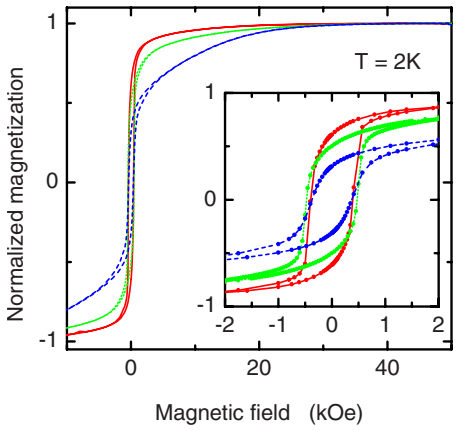

FIG. 7. (Color online) Magnetization normalized to the saturation value at a temperature of $T=2$ K. An external magnetic field is applied along the $[33\bar{2}]$ and $[\bar{1}10]$ directions of the substrate for the solid and dotted lines, respectively. For the dashed line, the in-plane field is inclined by 45° from the $[33\bar{2}]$ and $[\bar{1}10]$ directions. The hysteresis loops are shown with an expanded scale in the inset.

axes using superconducting quantum interference device magnetometer. We show in Fig. 7 the dependence of magnetization on an external magnetic field H when the field is aligned along three in-plane directions. The C plane is the magnetic easy plane for bulk MnAs and so the magnetocrystalline anisotropy in the structural domains is uniaxial. The magnetization curves when $H\|[33\bar{2}]$ (solid line) and $H\|[\bar{1}10]$ (dotted line) are interpreted as follows. The two structural domains provide identical contributions to magnetization in these cases. The magnetic field is inclined with respect to the magnetic easy axis by $\phi_{\text{tilt}}=48°$ and 42° when the field is along the $[33\bar{2}]$ and $[\bar{1}10]$ directions of the substrate, respectively. The magnetic moments thus flip at $H=\pm H_{c0}/\cos(\phi_{\text{tilt}})$, where H_{c0} is the coercive field when the field is in the direction of the magnetic easy axis. With further increasing $|H|$, the magnetic moments are gradually oriented toward the direction of the field and so the magnetization increases steadily until saturation is reached.

When the in-plane field is tilted by 45° from the $[\bar{1}10]$ and $[33\bar{2}]$ directions of the substrate, the field is nearly along the magnetic easy axis for one of the structural domains but approximately parallel to the magnetic hard axis for the other structural domain. Consequently, the magnetization curve is a superposition of the easy- and hard-axis behaviors, as shown by the dashed line in Fig. 7. Remanence is about half of the saturation magnetization, indicating that the volume fractions of the two domains are nearly the same. The variation in the magnetization characteristics with the direction of the external magnetic field thus evidences that there is no major contribution to the magnetization other than that from the crystal orientations shown in Fig. 6.

The magnetic easy axes in the two structural domains associated with the coexisting c-axis orientations are not orthogonal to each other. The magnetic dipole interactions between these domains are thus anticipated to be unconventional due to the plausible geometrical frustrations.[19] The coupling of an in-plane magnetization to an out-of-plane component has been demonstrated to be useful for magnetologic operations.[20] The unusual inclination angle between the magnetic moments in the $(21\bar{3}1)$-oriented MnAs layer may provide a new functionality for magnetologic devices, for instance, multilevel logics.

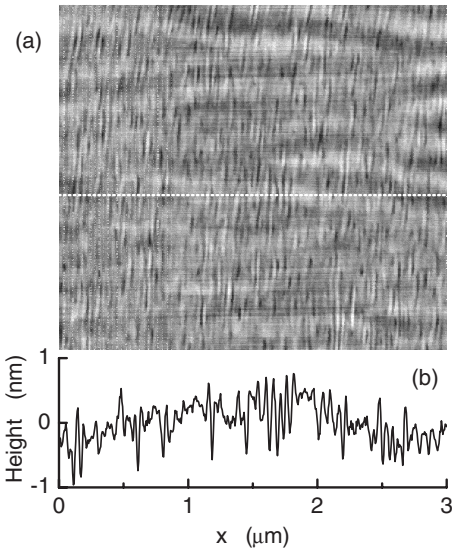

FIG. 8. (a) Atomic-force micrograph of a MnAs layer on GaAs(113)A grown by MBE, which is identical to that shown in Fig. 2(b). The $[1\bar{1}0]$ and $[33\bar{2}]$ directions of the substrate are aligned in the vertical and horizontal directions, respectively. The scan area is 3.0×2.7 μm^2. (b) Line scan at the position indicated by the dotted line in (a).

V. OVERGROWTH ON CORRUGATIONS

Let us finally remark on MnAs overgrowth on patterned substrates. The layer shown in Fig. 2(a) exhibits an additional stripe pattern which is orthogonal to the stripe of α- and β-MnAs, as shown by the atomic-force micrograph in Fig. 8(a). The short-period stripe is a remnant of the corrugations that are characteristic for the GaAs(113)A surface.[21] Similar stripes on the GaAs(113)B surface are clearly visible in Figs. 2(b) and 2(d). The line scan plotted in Fig. 8(b) shows that the amplitude of the short-period height modulation is 0.5–1.0 nm. Therefore, the original corrugations on the GaAs(113) surface are seen to be almost completely preserved even after the overgrowth of a 50-nm-thick MnAs layer.[22]

In as-grown MnAs layers on GaAs(331)B, the hysteresis loops in the magnetization and resistance around T_C associated with the first-order phase transition are drastically altered by initial thermal cycles.[23] The permanent alteration of the hysteresis loops is driven by the nonplanar phase-transition stress resulting from the zigzag shape of the step bunching that emerged on the GaAs(331)B surface during the growth of the GaAs buffer layer. We have confirmed that the corrugations on the GaAs(113) surface do not give rise to such an alteration of the hysteresis loops. As the amplitude of the corrugations on the GaAs(113) surface is about one order

of magnitude smaller than that of the step bunching on the GaAs(331) surface, the out-of-plane component of the phase-transition stress appears to be negligibly small.

VI. CONCLUSIONS

In conclusion, we have compared the MnAs layers on GaAs(113)A and GaAs(113)B grown by means of conventional molecular-beam epitaxy and solid-phase epitaxy. The layers grown on the A surface using solid-phase epitaxy have been found to be highly unusual. That is, the surface orientation is $(21\bar{3}1)$ and the c axis of MnAs is tilted in the surface plane by about $\pm 42°$ with respect to the GaAs$[33\bar{2}]$ direction in an asymmetric manner. We have shown that the reduction in the strain energy is responsible for the generation of such a low-symmetry crystal orientation. The bonding energy gives rise to a partial absence of the symmetries among the coexisting crystal orientations due to the in-plane polarization in the GaAs(113) surface. The strain-favored epitaxial orientation is not realized when MnAs layers are grown on the B surface, indicating that the energy associated with the atomic bonding at the heterointerface is more important on the B surface than on the A surface. In order to clarify the role of the bonding energy, first-principle calculations are needed. The calculations are demanded to reproduce the consequences of the bonding energy in both the missing symmetries and the difference in generating the low-symmetry $(21\bar{3}1)$ orientation between the A and B surfaces of GaAs(113).

[1] I. Žutić, J. Fabian, and S. Das Sarma, Rev. Mod. Phys. **76**, 323 (2004).
[2] M. Tanaka, Semicond. Sci. Technol. **17**, 327 (2002).
[3] L. Däweritz, Rep. Prog. Phys. **69**, 2581 (2006).
[4] M. Ramsteiner, H. Y. Hao, A. Kawaharazuka, H. J. Zhu, M. Kästner, R. Hey, L. Däweritz, H. T. Grahn, and K. H. Ploog, Phys. Rev. B **66**, 081304(R) (2002).
[5] P. N. Hai, Y. Sakata, M. Yokoyama, S. Ohya, and M. Tanaka, Phys. Rev. B **77**, 214435 (2008).
[6] J. Stephens, J. Berezovsky, J. P. McGuire, L. J. Sham, A. C. Gossard, and D. D. Awschalom, Phys. Rev. Lett. **93**, 097602 (2004).
[7] S. Gama, A. A. Coelho, A. de Campos, A. M. G. Carvalho, F. C. G. Gandra, P. J. von Ranke, and N. A. de Oliveira, Phys. Rev. Lett. **93**, 237202 (2004).
[8] Y. Takagaki and K.-J. Friedland, J. Appl. Phys. **101**, 113916 (2007).
[9] V. Garcia, Y. Sidis, M. Marangolo, F. Vidal, M. Eddrief, P. Bourges, F. Maccherozzi, F. Ott, G. Panaccione, and V. H. Etgens, Phys. Rev. Lett. **99**, 117205 (2007).
[10] Y. Takagaki, C. Herrmann, J. Herfort, C. Hucho, and K.-J. Friedland, Phys. Rev. B **78**, 235207 (2008).
[11] Y. Takagaki, C. Herrmann, B. Jenichen, J. Herfort, and O. Brandt, Appl. Phys. Lett. **92**, 101918 (2008); Appl. Phys. Lett. **92**, 179901 (2008).
[12] Y. Takagaki, C. Herrmann, B. Jenichen, and O. Brandt, Phys. Rev. B **78**, 064115 (2008).
[13] C. Setzer, J. Platen, W. Ranke, and K. Jacobi, Surf. Sci. **419**, 291 (1999).
[14] J. Platen, A. Kley, C. Setzer, K. Jacobi, P. Ruggerone, and M. Scheffler, J. Appl. Phys. **85**, 3597 (1999).
[15] R. P. Panguluri, G. Tsoi, B. Nadgorny, S. H. Chun, N. Samarth, and I. I. Mazin, Phys. Rev. B **68**, 201307(R) (2003).
[16] G. Kirczenow, Phys. Rev. B **63**, 054422 (2001).
[17] L. Wan, J. Shangguan, H. Luo, Y. Huang, and B. Tang, Eur. Phys. J.: Appl. Phys. **38**, 231 (2007).
[18] I. Galanakis, G. Bihlmayer, V. Bellini, N. Papanikolaou, R. Zeller, S. Blügel, and P. H. Dederichs, Europhys. Lett. **58**, 751 (2002).
[19] Y. Takagaki, C. Herrmann, E. Wiebicke, J. Herfort, and B. Jenichen, J. Appl. Phys. **101**, 123914 (2007).
[20] C. Pampuch, A. K. Das, A. Ney, L. Däweritz, R. Koch, and K. H. Ploog, Phys. Rev. Lett. **91**, 147203 (2003).
[21] M. Wassermeier, J. Sudijono, M. D. Johnson, K. T. Leung, B. G. Orr, L. Däweritz, and K. Ploog, Phys. Rev. B **51**, 14721 (1995).
[22] K. Jang, Y. Okada, and M. Kawabe, Jpn. J. Appl. Phys. **39**, 4266 (2000).
[23] Y. Takagaki, C. Herrmann, B. Jenichen, and J. Herfort, Phys. Rev. B **79**, 235320 (2009).